Interactions of fast HeH^+ beams with matter

P. J. Cooney,* D. S. Gemmell, W. J. Pietsch,† A. J. Ratkowski,‡ Z. Vager,§ and B. J. Zabransky
Physics Division, Argonne National Laboratory, Argonne, Illinois 60439
(Received 4 December 1980)

We present experimental results from high-resolution studies of the energy and angle distributions for the breakup products that arise from the dissociation of fast-moving $^4HeH^+$ and $^3HeH^+$ in thin carbon foils. These results are compared with calculations based on a model for the polarization "wakes" induced in foils by the passage of fast charged projectiles. We also describe measurements on the transmission of such fast molecular ions through thin foils and present results on the transmission probabilities, energy losses, and angular distributions of the transmitted ions. A mechanism is proposed to account for these observations on molecular-ion transmission. Related studies on the foil-induced dissociation of OH^+, OH_2^+, CH^+, H_2^+, and $^3He_2^+$ are also briefly reported.

I. INTRODUCTION

In recent publications[1-11] we have reported new effects seen in high-resolution measurements of the distributions in angle and in energy for the breakup fragments produced when fast molecular-ion beams ($2 \lesssim v/v_0 \lesssim 10$, where $v_0 = e^2/\hbar$) bombard thin foil targets or gas targets. These effects manifest themselves in pronounced departures from what one might expect based on a simple "Coulomb-explosion" picture in which a cluster of nuclei, stripped of their binding electrons, moves apart under the influence of their mutual Coulomb repulsion. In the case of solid targets, an explanation for these differences has been offered in terms of an interaction between the projectiles and the electronic polarization induced in the target by their passage. A theoretical model describing this interaction has been developed.[12] Calculations based on this model reproduced the main features of the experimental results obtained for the dissociation of fast $^4HeH^+$ ions in thin carbon foils.

We present here the results of a study on the dissociation of energetic (up to 4 MeV) beams of $^4HeH^+$ and $^3HeH^+$ in carbon foils. This study was performed with a view of test the theoretical model in a detailed way and to explore its limitations. To this end, we have varied such parameters as the beam velocity, the target thickness, and the isotopic composition of the molecular ions. We have also made measurements for a variety of charge states of the dissociation products H^+, H^0, H^-, He^{++}, He^+, and He^0). A related study reported here concerns the transmission of $^4HeH^+$ and $^3HeH^+$ through carbon foils. We have measured the transmitted fractions, energy losses, and angular distributions for various bombarding energies and target thicknesses.

The HeH^+ molecular ion was chosen for this study because it is one of the lightest, structurally simple, heteronuclear, diatomic ions readily available as a beam from an accelerator. The relatively big differences in mass and charge of the two nuclei result in large and easily observable polarization "wake" effects. The light mass permits measurements at high velocity (where the projectile nuclei are almost fully stripped of electrons) with modest accelerator voltages.

II. EXPERIMENTAL ARRANGEMENT

Magnetically analyzed HeH^+ beams from Argonne's 4-MV Dynamitron accelerator were collimated to have a maximum angular divergence of ± 0.09 mrad at the target position (Fig. 1). The ions were produced in the accelerator terminal from a duo-plasmatron ion source fed with a mixture of 90% He and 10% H_2. A set of "predeflector" plates permitted electrostatic deflection of the beam incident on the target. Similarly, a set of "postdeflectors" was used to deflect charged particles emerging from the target. Charged particles entering the electrostatic analyzer were energy-analyzed with a relative resolution of $\pm 3 \times 10^{-4}$. The angular acceptance of the analyzer was ± 0.11 mrad. Distributions in angle and energy were made for particles emerging from the target, by varying the voltages on the predeflector and/or the postdeflector in conjunction with those on the analyzer Neutrals were energy analyzed by first stripping them in a ~100-Å-thick carbon foil located just

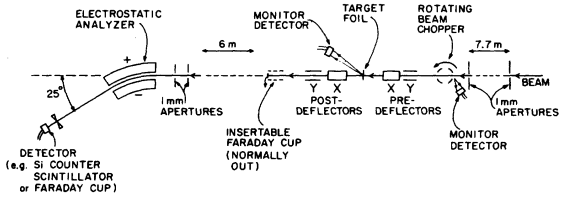

FIG. 1. Schematic experimental arrangement used at Argonne's 4-MV Dynamitron accelerator.

ahead of the analyzer (the stripping did not introduce a significant degradation in energy resolution). The overall angular resolution was ± 0.15 mrad (0.008°). Selection of the required charge state for particles leaving the target was facilitated by a suitable combination of pre- and postdeflection. The optimal combination also rejected spurious incident beams (e.g., predissociated fragments arising from interactions in residual gas upstream from the target). Elaborate precautions were taken to ensure negligible carbon buildup on the target foils. These precautions included heating the targets to ~150°C and surrounding them with a liquid-nitrogen cooled copper shield that contained small apertures to permit the passage of beam particles. Gas target experiments were performed by removing the foil target and flooding the entire target chamber with gas (typically to a pressure of $\sim 10^{-5}$ Torr). Appropriate voltages on the deflectors were then used to restrict the viewed region of interaction to that between the inner two sets of x-deflection plates.

III. THE DISSOCIATION OF HeH+ IN CARBON FOILS

A. Expectations based on a simple Coulomb-explosion model

When a fast (for example, 2-MeV) HeH+ projectile is incident upon a solid target, the two electrons that bind the molecular ion are expected to be stripped off almost always within a few angstroms of penetration into the target. This is a consequence of the large cross sections ($\sim 10^{-16}$ cm^2/atom for electron loss due to collisions with target electrons. This is also consistent with recent measurements[13] showing that two such binding electrons only remain correlated with the incident ion for a few times 10^{-17} sec after entering the foil target. It is therefore reasonable to assume that the projectile's electrons are removed instantaneously at the moment of entrance into a carbon foil target. This allows us to make simple estimates of the magnitudes of quantities (energies, angles, times, etc.) involved in the breakup of the molecular projectile.

Figure 2 shows the solution, $r(t)$, to the equation of motion ($\mu\ddot{r} = Z_1 Z_2 e^2/r^2$) governing the simple Coulomb explosion of the ^{4}HeH+ molecular ion. Here $r(t)$ is the internuclar separation at time t and μ is the reduced mass of the α particle and proton combination. For the purposes of Fig. 2, which is designed merely to illustrate the times and distances involved, we assume $Z_1 = 1$, $Z_2 = 2$, $\dot{r}(0) = 0$, and $r_0 = r(0) = r_e$, the equilibrium separation in the electronic ground state. (For HeH+, r_e has been calculated[14] to be 0.774 Å.)

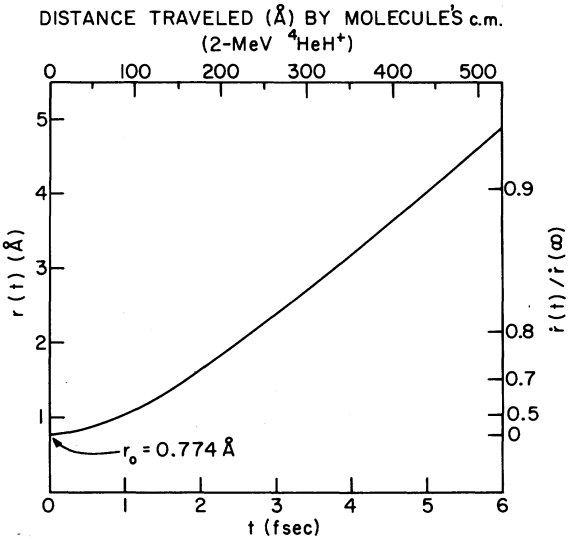

FIG. 2. Time development of the simple Coulomb explosion of the nuclei in ^{4}HeH+. The top scale gives the distance traveled by the beam in times corresponding to the bottom scale assuming a beam energy of 2.0 MeV.

Å.) With these assumptions, the time for the internuclear distance to increase by a factor ξ is easily shown to be

$$t(\xi) = (\mu r_0^3/2Z_1Z_2e^2)^{1/2}\{[\xi(\xi-1)]^{1/2} + \ln(\sqrt{\xi}+\sqrt{\xi-1})\}. \quad (1)$$

From this it can be seen that the initial potential energy is converted into kinetic energy in times on the order of a few femtoseconds (fsec). In these times, the projectile typically travels a few hundred angstroms. The final relative velocity of separation is given by $u = \dot{r}(\infty) = (2Z_1Z_2e^2/\mu r_0)^{1/2}$. For the case shown in Fig. 2, $u = 9.5 \times 10^6$ cm/sec, which is about 1% of the incident beam velocity, v ($v = 8.8 \times 10^8$ cm/sec for 2-MeV HeH+).

With these simplifying assumptions, one readily calculates that the protons from the dissociation of 2-MeV HeH+ may be observed in the laboratory system (at times $t \gg 10^{-15}$ sec.) to have a maximum angular deviation from the beam direction of approximately $\pm(M_\alpha Z_1 Z_2 e^2/M_p r_0 E)^{1/2} \approx \pm 8.6$ mrad (0.49°), where E is the beam energy and M_α and M_p are the masses of the α particle and proton, respectively. This maximum deviation corresponds to the molecular axis being normal to the beam direction and there is then approximately zero energy shift due to the Coulomb explosion. Similarly, when the molecular axis is parallel to the beam direction, there is no angular shift, but the energy shift has the maximum value of approximately $\pm[4M_pM_\alpha Z_1 Z_2 e^2 E/r_0(M_p+M_\alpha)^2]^{1/2}$

$\approx \pm 6.9$ keV. The positive sign refers to the case when the proton leads the α particle and the negative sign to the proton trailing. The maximum energy shift for the α particle has the same value, but the maximum angular deflection is about a factor of 4 smaller.

It can be expected that the HeH^+ ions in the incident beam are to be found in a range of vibrationally and rotationally excited states. The nuclear velocities associated with these excitations are small compared with the c.m. velocities ($\sim 10^7$ cm/sec) acquired as a result of the molecular Coulomb explosions and we may, as a first approximation, ignore them. However, molecular vibrations also have the consequence that at the instant of electron removal the internuclear separation can have a value that lies anywhere within a wide range of possible values. This then gives rise to a range of possible Coulomb explosion energies.

Figure 3 illustrates the calculated "ring" pattern predicted on the basis of the simplified picture of the Coulomb explosion outlined above. The calculation pertains to protons from the breakup of 2-MeV HeH^+ in a thin (85-Å) carbon foil. We

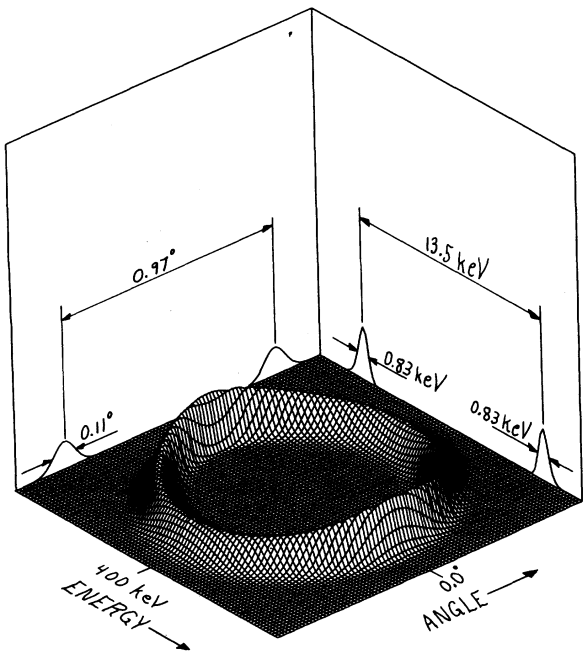

FIG. 3. Joint distribution in energy and angle (relative to the beam direction) expected for protons arising from the simple Coulomb explosion of $^4HeH^+$ ions incident at an energy of 2 MeV. The Coulomb explosion is assumed to start at the entrance surface of an 85-Å-thick carbon foil. The two single-parameter distributions shown are those for zero shift in energy and angle. They thus correspond to cuts (a "cross") through the center of the ring pattern.

have ignored the small (less than 1-keV) energy loss of the protons due to the stopping power of the foil. In the calculation it is assumed that r_0 is distributed as a Gaussian ($\sigma = 0.081$ Å) about r_e (this ought to be reasonably accurate for the case where the incident ions are in the ground vibrational state). The calculation includes the effects of multiple scattering [multiple scattering contributes 1.6 mrad (0.09°) FWHM to the angular width], but omits any energy straggling effects (these are expected to be negligibly small). The diameters of the ring (0.97° and 13.5 keV) measure between the maxima are slightly lower than the values (0.99° and 13.8 keV) calculated above for fixed $r_0 = r_e$. This is a consequence of r_0 now assuming a range of values due to molecular vibrations.

B. Observed distributions of fragments from the dissociation of HeH^+

Most of our data on the dissociation fragments produced from molecular-ion beams take the form of measurements of either a complete "ring" pattern (i.e., a joint energy-angle distribution) or a "cross" [i.e., an energy distribution for zero angular shift together with an angular distribution for zero energy shift (allowing for the usually small energy loss due to the stoppin power of the target)]. Figures 4 and 5 show examples for protons from $^4HeH^+$. The smooth curve drawn through these and all subsequent dissociation data presented as "crosses" are simply to guide the eye.

A comparison of Figs. 3 and 4 illustrates the significant departures of the observed results from those expected on the basis of a simple Coulomb explosion. These differences have been accounted for[3,12] in terms of the interaction between a fragment and the polarization "wake" induced in the foil by its partner fragment. The wake, which has been discussed by several authors,[12,15-21] represents the response of the target electrons to the passage of a fast charged projectile. Following the treatment of Ref. 12, the target can be considered as an electron gas, in which the projectile induces regions of alternately enhanced and depleted electron density that trail behind it. Figures 6 and 7 show examples of the wake potential calculated with such a model, and of the resulting computer-calculated ring pattern corresponding to the data in Fig. 4. In calculating the ring shown in Fig. 7, the distribution of internuclear separations in the incident HeH^+ beam was taken to be Gaussian, with a mean value $r_0 = 0.79$ Å and $\sigma = 0.15$ Å. The generally good agreement between the calculated and

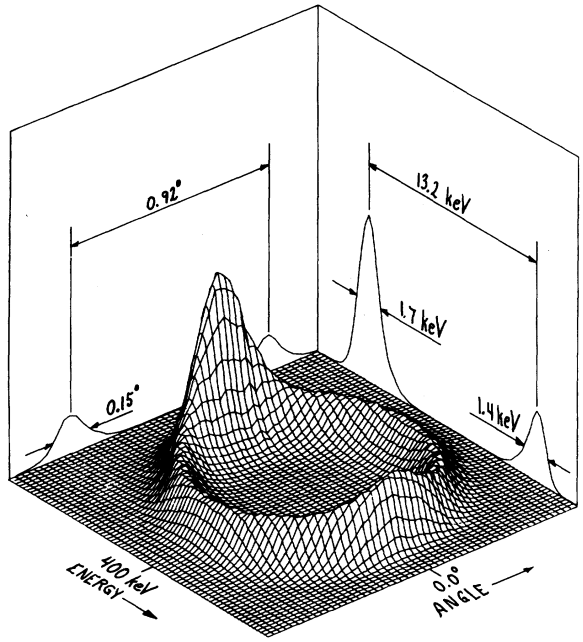

FIG. 4. "Ring" pattern (see text) measured for protons emerging from an 85-Å carbon foil bombarded by 2.0-MeV $^4HeH^+$ ions. There are about 10 000 counts in the highest peak.

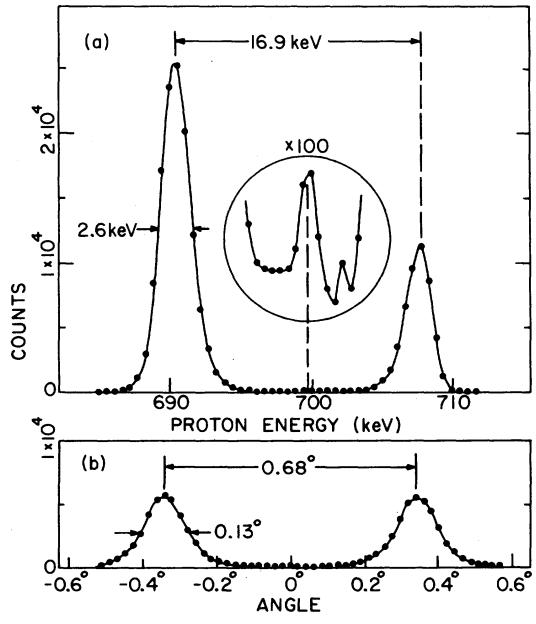

FIG. 5. "Cross" (see text) measured for the protons arising from 3.5-MeV $^4HeH^+$ ions bombarding a 200-Å-thick carbon foil.

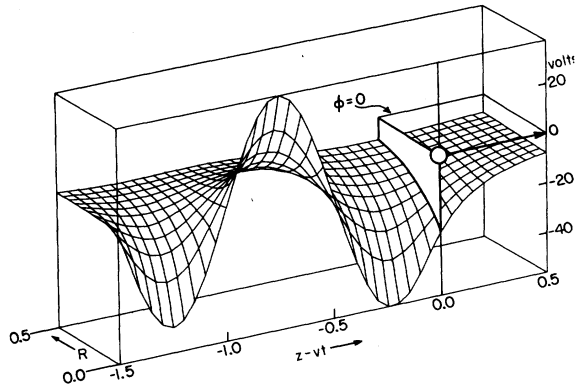

FIG. 6. Potential distribution associated with the polarization wake of a 400-keV proton traversing carbon. The ion track is along the Z axis and R is the radial distance. Distances are shown in units of $\lambda = 14.5$ Å (Ref. 12).

measured ring parameters would suggest that the incident HeH^+ ions are mostly in the lowest few vibrational levels of the molecular ion. A more detailed presentation of the use of such ring patterns to determine the distribution of internuclear separations in a beam of molecular ions has been published separately.[4]

In Fig. 8 we show "crosses" measured for H^+,

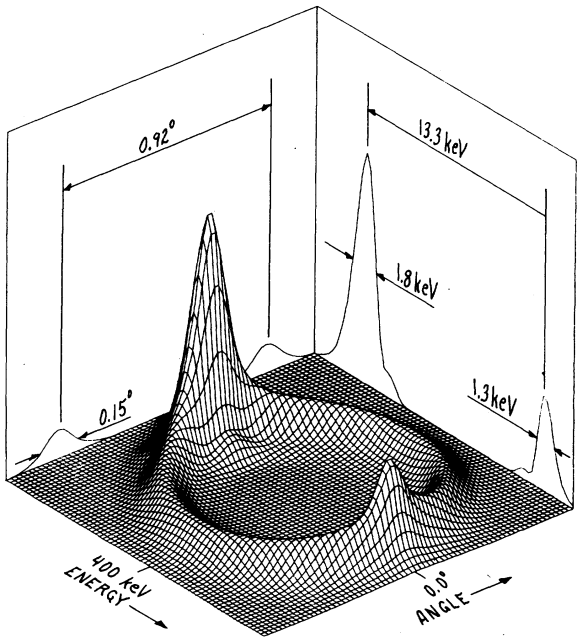

FIG. 7. Calculated "ring" pattern for protons emerging from an 85-Å carbon foil bombarded by 2.0-MeV $^4HeH^+$ (cf. Fig. 4). In the calculation, the hydrogen ions are assumed to be singly charged both inside the target foil and after leaving it. The helium ions are assumed to be doubly charged inside the foil and 92% doubly and 8% singly charged after emergence from the foil (Ref. 22).

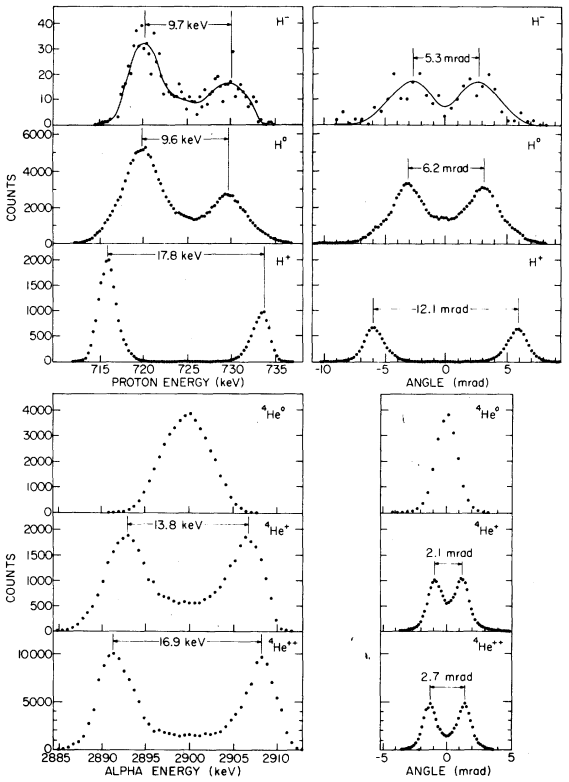

FIG. 8. "Crosses" for H^-, H^0, H^+, $^4He^0$, $^4He^+$, and $^4He^{++}$ arising from 3.63-MeV $^4HeH^+$ ions bombarding a 160-Å-thick carbon foil.

H^0, H^-, He^0, He^+, and He^{++} ions arising from the bombardment of a 160-Å carbon foil by 3.63-MeV $^4HeH^+$. An example of the dependence upon target thickness is given in Fig. 9 for the case of H^0 coming from the breakup of 3.63-MeV $^4HeH^+$. Figure 10 compares "crosses" measured for protons from $^4HeH^+$ and $^3HeH^+$ ions of the same velocity. The dependences of ΔE and $\Delta\theta$, the separations in energy and angle of the peaks in the "crosses," upon target foil thickness and incidence velocity are shown in Fig. 11 for various breakup products from $^4HeH^+$.

Table I shows a comparison of the measured and calculated values of ΔE and $\Delta\theta$, the separations in energy and angle, respectively, of the peaks in the "crosses" for 3.63-MeV $^4HeH^+$ and 2.9-MeV $^3HeH^+$ dissociating in a 100-Å carbon foil. Table II gives a similar comparison for a range of target thicknesses and bombarding energies for $^4HeH^+$. The overall agreement is good.

For H^- (Fig. 8), the observed values of ΔE and $\Delta\theta$ and the general shapes of the "crosses" are about the same as for H^0. Since H^0 and H^- are well separated by our postdeflection system, this result indicates that the H^- ions leave the target

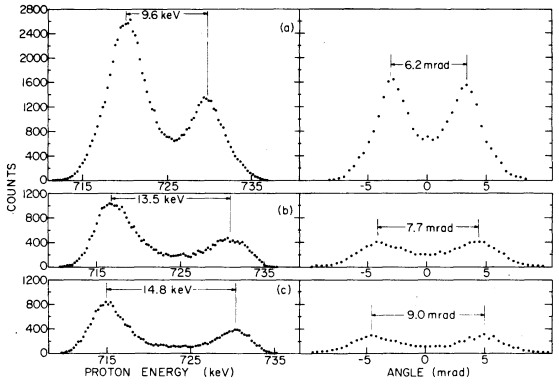

FIG. 9. "Crosses" for H^0 arising from 3.63-MeV $^4HeH^+$ ions bombarding carbon foils with thicknesses (a) 3.2, (b) 7.2, and (c) 10.4 $\mu g/cm^2$. The data are normalized for equal numbers of incident $^4HeH^+$ ions.

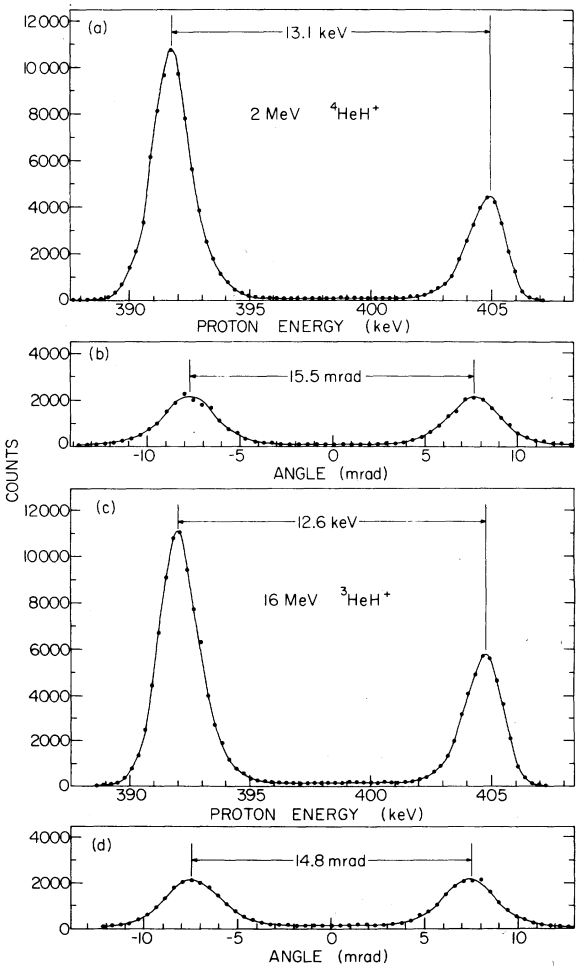

FIG. 10. "Crosses" measured for protons arising from (a) 2.0-MeV $^4HeH^+$ and (b) 1.6-MeV $^3HeH^+$ ions bombarding a 160-Å-thick carbon foil.

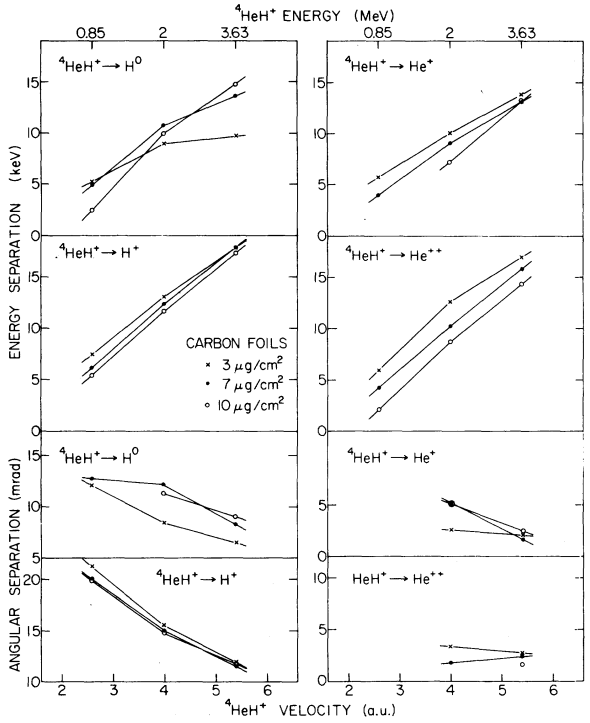

FIG. 11. Velocity dependences of the separations in energy (ΔE) and angle ($\Delta\theta$) of the peaks seen in "crosses" for H^0, H^+, $^4He^+$, and $^4He^{++}$ arising from $^4HeH^+$ ion bombardment of carbon foils with thicknesses 3, 7, and 10 $\mu g/cm^2$. The straight lines merely indicate trends in these data.

as H^0 and then at some later time (10^{-15} sec $\ll t \ll 10^{-9}$ sec) capture an electron. The most likely source of that electron is the partner He ion which may be in some excited state and able to shed an electron. The lifetime of this state may be long compared with the Coulomb explosion time, but short compared with the flight time to the postdeflectors.

TABLE I. Comparison of experimental and calculated results for dissociation products from 3.63-MeV $^4HeH^+$ and 2.9-MeV $^3HeH^+$ bombarding a 160-Å carbon foil.

Outgoing particle	3.63-MeV $^4HeH^+$ ΔE (keV)	3.63-MeV $^4HeH^+$ $\Delta\theta$ (mrad)	2.9-MeV $^3HeH^+$ ΔE (keV)	2.9-MeV $^3HeH^+$ $\Delta\theta$ (mrad)
H^0 Expt.	9.7	6.5	9.4	5.9
Calc.	9.7	5.8	9.6	5.8
H^+ Expt.	17.8	11.9	17.2	11.4
Calc.	18.0	12.1	17.4	11.8
He^0 Expt.	One peak		One peak	
Calc.	8.7	1.3	8.7	1.8
He^+ Expt.	13.8	2.1	12.9	2.8
Calc.	14.0	2.4	13.6	3.1
He^{++} Expt.	16.9	2.7	16.7	3.7
Calc.	17.5	3.0	16.9	3.9

IV. WORK WITH OTHER MOLECULAR-ION BEAMS

Figures 12–14 show some representative examples of results obtained for the foil dissociation of molecular ions other than HeH^+. A comparison between the experimental and calculated results is given in Table III for some of the molecular dissociations discussed here and shown in the various figures. It can be seen from Table III that the values of $\bar{r}_0$ required to fit the experimental data all lie close to their corresponding value of r_e. This suggests that the molecules incident on the target are almost always in their ground vibrational states. It is a reasonable assumption that many of these molecular ions would be produced in the ion source in such a way

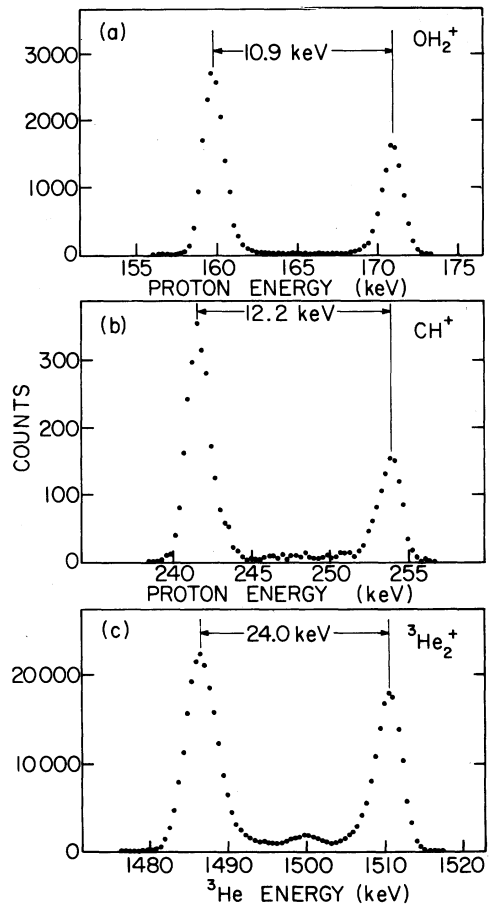

FIG. 12. Zero-angle energy spectra for (a) protons from 2.97-MeV OH_2^+ bombardment of a 2.4-$\mu g/cm^2$ carbon foil, (b) protons from 3.25-MeV CH^+ bombardment of a 2-$\mu g/cm^2$ carbon foil, and (c) $^3He^{++}$ ions from 3.0-MeV $^3He_2^+$ bombardment of a 2.5-$\mu g/cm^2$ carbon foil.

TABLE II. Comparison of measured and calculated results for the breakup fragments produced in the foil-induced dissociation of $^4HeH^+$.

Target	Detected particle	0.85-MeV $^4HeH^+$ ΔE (keV) Calc.	Expt.	$\Delta\theta$ (mrad) Calc.	Expt.	2.0-MeV $^4HeH^+$ ΔE (keV) Calc.	Expt.	$\Delta\theta$ (mrad) Calc.	Expt.	3.63-MeV $^4HeH^+$ ΔE (keV) Calc.	Expt.	$\Delta\theta$ (mrad) Calc.	Expt.
3.3 $\mu g/cm^2$ carbon	H^0	4.1	5.2	7.4	12.1	7.9	9.0	8.1	8.4	9.7	9.7	5.8	6.5
	H^+	7.5	7.5	17.6	21.3	13.0	13.1	15.5	15.5	18.0	17.8	12.1	11.9
	$^4He^0$	3.8				7.4		1.9		8.7		1.3	
	$^4He^+$	5.9	5.7	3.7		10.4	10.1	3.1	2.6	14.0	13.8	2.4	2.1
	$^4He^{++}$	7.5	6.0	4.9		12.7	12.6	3.9	3.3	17.5	16.9	3.0	2.7
7 $\mu g/cm^2$ carbon	H^0	5.1	4.9	9.2	12.7	10.1	10.7	10.6	12.1	14.3	13.7	8.7	8.2
	H^+	6.7	6.2	14.1	20.1	12.3	12.3	14.1	15.0	17.9	17.9	11.7	11.5
	$^4He^0$	4.9				9.8		2.4		13.6		2.1	
	$^4He^+$	5.7	3.9			10.9	9.0	3.0	5.1	16.6	13.1	2.5	1.6
	$^4He^{++}$	6.5	4.3	3.5		12.0	10.2	3.5	1.7	17.4	15.7	2.9	2.4
10 $\mu g/cm^2$ carbon	H^0	5.4	2.5	9.9		10.4	10.0	10.9	11.3	15.2	13.7	9.3	8.2
	H^+	7.9	5.4	13.0	11.9	11.9	11.6	13.4	14.7	17.7	17.3	11.5	11.8
	$^4He^0$	5.2				10.1				14.6		2.2	
	$^4He^+$	5.6				11.1	7.2	2.9	5.1	15.9	13.2	2.5	2.5
	$^4He^{++}$	6.3	2.2			11.7	8.7	3.2		17.1	14.3	2.8	1.6

that they populate a range of excited vibrational states. One would expect these states to have natural lifetimes in the millisecond range, i.e., long compared with the flight time from the ion source to the target which is typically microseconds. The reason for the depletion of excited states for the beam arriving at the target is uncertain but probably it is caused by collisional deexcitation and dissociation. These processes can reasonably be expected to be more pronounced for more highly excited states. We have certainly noticed the rapid disappearance of molecular beams if the accelerator vacuum is allowed to deteriorate. There may also be a large degree of collisional deexcitation in the narrow exit canal of the ion source.

The values of Z_1 and Z_2 (inside the target) used in the calculation are those required to fit the stopping powers. The calculated values of ΔE and $\Delta\theta$ (Table III) agree well with the measured values with the notable exception of those for neutral hydrogen atoms detected from OH^+. This indicates that an after-foil repulsion occurs via

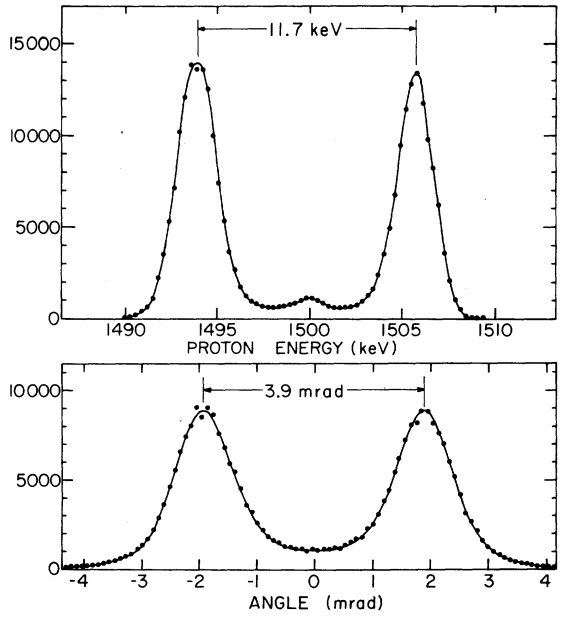

FIG. 13. "Cross" for protons arising from 3.0-MeV H_2^+ bombardment of a 3.3-$\mu g/cm^2$ carbon foil.

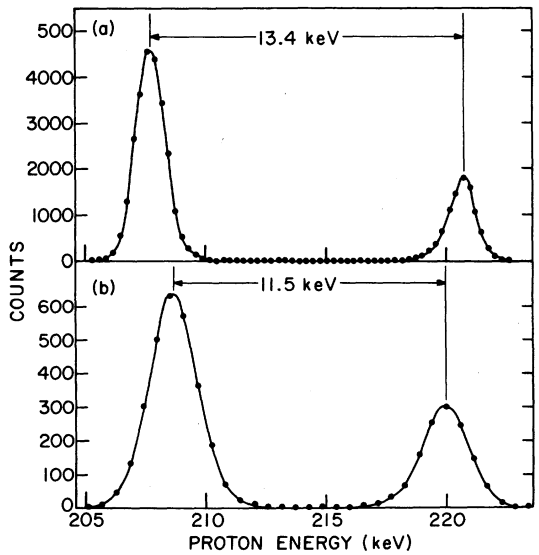

FIG. 14. Zero-angle energy spectra for (a) protons and (b) H^0 from 3.7-MeV OH^+ bombardment of a 3.3-$\mu g/cm^2$ carbon foil.

TABLE III. Comparison of experimental and calculated results for the dissociation of various molecular ions in carbon foils.

Molecular ion	Beam energy (MeV)	Detected ion	Figure no.	ΔE (keV) Expt.	ΔE (keV) Calc.	Δθ (mrad) Expt.	Δθ (mrad) Calc.	r_e (Å)	$\bar{r}_0$ (Å)	Z_1Z_2 (inside target)
H_2^+	3.0	H^+	13	11.7	11.5	3.9	3.9	1.06	1.08	1.00
$^3HeH^+$	1.6	H^+	10	12.6	12.5	14.8	15.1	0.77	0.79	1.78
$^4HeH^+$	2.0	H^+	10	13.1	13.0	15.5	15.5	0.77	0.79	1.79
$^3He_2^+$	3.0	$^3He^{++}$	12	24.0	24.2	7.5	8.1	1.08	1.10	3.72
CH^+	3.25	H^+	12	12.2	12.7			1.13	1.15	2.86
OH^+	3.7	H^0	14	11.5	7.0	21.5	10.4	1.03	1.05	3.05
OH^+	3.7	H^+	14	13.4	12.6	28.6	24.9	1.03	1.05	3.05

dissociative molecular states associated with the neutral hydrogen. The role of such molecular states has been examined in a previous publication.[4]

V. THE TRANSMISSION OF HeH$^+$ THROUGH CARBON FOILS

In 1971 Poizat and Remillieux[23] demonstrated the rather remarkable fact that there is a small but significant probability for 2-MeV H_2^+ ions to be transmitted through thin carbon foils. We have observed that $^4HeH^+$ and $^3HeH^+$ ions are also transmitted and we have measured the transmission probability T, the energy loss, and the angular distributions for transmitted ions over a range of target thicknesses and bombarding energies. Figure 15 illustrates a typical energy-loss spectrum and angular distribution. Figures 16–20 show data obtained in our various transmission measurements. We have also made one measurement on the transmission of 2-MeV H_2^+ through an 11-μg/cm^2 carbon foil and for this our value of $T = 1.4 \times 10^{-5}$ is in reasonable agreement with that of the Lyon group[24] ($T = 1.2 \times 10^{-5}$).

In contrast with results obtained[24-26] for H_2^+, the transmission yield of $^4HeH^+$ for a given target thickness is strongly energy dependent (Figs. 16 and 18). Other measurements[25] with 300-keV $^4HeH^+$ have shown no detectable transmission (i.e., $T < 10^{-7}$) even for the thinnest carbon targets used (6 μg/cm^2). This result, is taken in conjunction with the data reported here, indicates that the transmission yield must drop by at least a factor of 20 as the bombarding energy is reduced from 800 to 300 keV. The implied sudden reversal of the energy dependence observed in our results warrants further investigation.

Comparison of the transmission for 3.0-MeV $^4HeH^+$ and 2.4-MeV $^3HeH^+$ is of interest. At the velocity corresponding to these energies, both the He and H ions should be almost fully stripped. This means that the decelerations for $^4He^{++}$ and H^+ due to the target's stopping power should be almost identical. On the other hand, the $^3He^{++}$ ions should decelerate more rapidly than their partner H^+ and one might conjecture that this should result in markedly reduced transmission as compared with the $^4HeH^+$ case—especially for thicker targets. This type of argument has been advanced[25] to explain the enormously different behaviors of the transmission yields for H_2^+ and HD^+ as functions of the target thickness. In striking contrast to the H_2^+ and HD^+ cases, the transmission yield for $^3HeH^+$ is not much lower

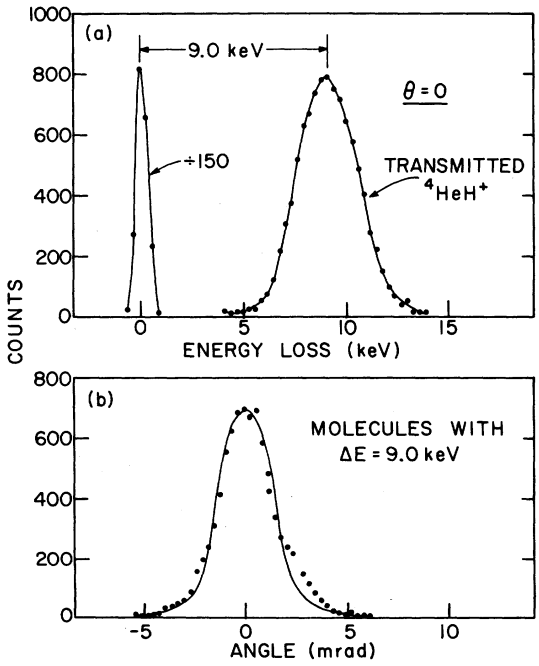

FIG. 15. (a) Energy-loss spectrum and (b) angular distribution for 1.2-MeV $^4HeH^+$ ions transmitted through a 3.7-μg/cm^2 carbon foil. The peak at $\Delta E = 0$ is due to ions transmitted through pin holes in the target foil.

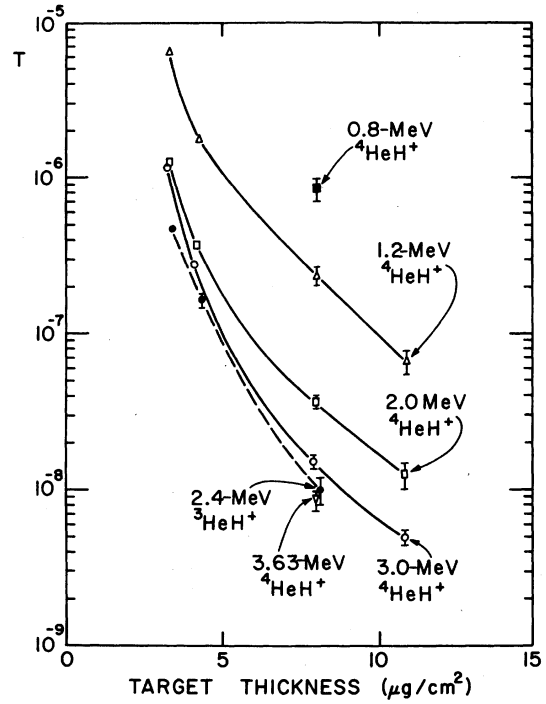

FIG. 16. Transmission yield as a function of carbon target thickness for HeH^+ ions. In this figure, as well as the next two figures, the smooth curves merely serve to guide the eye.

(typically only a factor of 2 or less) than that for $^4HeH^+$ and shows a very similar dependence on target thickness (Fig. 16).

As can be seen from Fig. 2, for target dwell

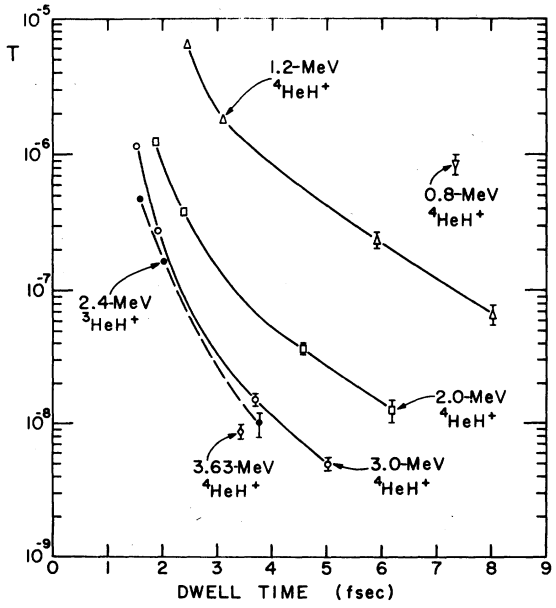

FIG. 17. Transmission yield as a function of target dwell time for HeH^+ ions.

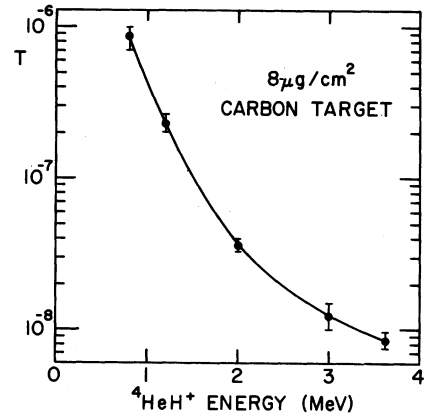

FIG. 18. The transmission yield as a function of bombarding energy for $^4HeH^+$ ions incident upon an 8-$\mu g/cm^2$ carbon foil.

times typical of our experiments (e.g., 5 fsec) the internuclear distance in a Coulomb exploding $^4HeH^+$ ion reaches about 4 Å and the relative velocity of separation is already about 90% of the final value. It is therefore difficult to see how a transmitted molecule could arise from the capture of two electrons at the foil exit by such a pair of rapidly separating nuclei. We therefore surmise that the transmission occurs only for incident projectiles whose initial internuclear separations are large. Figure 21 shows in more detail how initial values of r_0 develop in the first few fsec of the Coulomb explosion.

If we make the approximation that the transmission can be expressed as the product of two

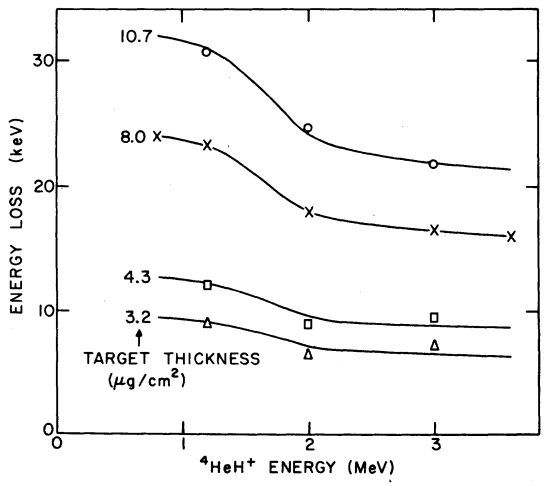

FIG. 19. The energy loss shown as a function of bombarding energy for $^4HeH^+$ ions transmitted through carbon foils. The solid line shown for the 8-$\mu g/cm^2$ target is a fit to the experimental points and the lines drawn for the remaining targets are then obtained by normalization according to target thickness.

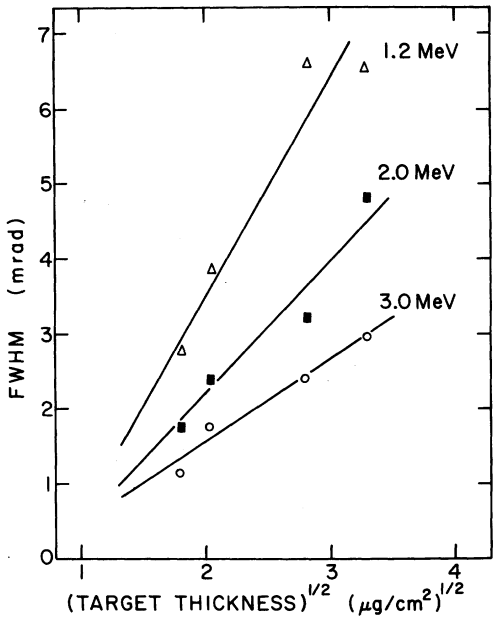

FIG. 20. Widths (FWHM) of the angular distributions measured for $^4HeH^+$ ions transmitted through carbon foils. The data are shown plotted versus the square root of the target thickness.

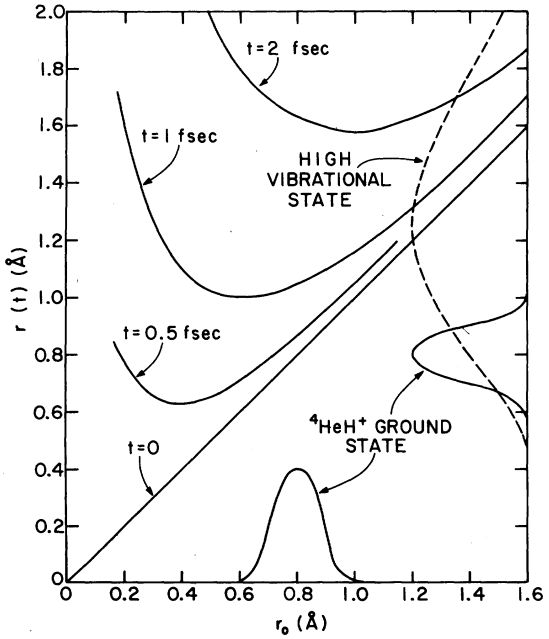

FIG. 21. Plot of the internuclear separation $r(t)$ as a function of $r_0 = r(0)$ for the Coulomb explosion of $^4HeH^+$. The distributions of r are given schematically for the ground vibrational state and for some postulated high vibrational state (or set of states). It is assumed here that $\dot{r}(0) = 0$ and that $Z_1 Z_2 = 2$.

probabilities, one $P(t)$ depending on the dwell time t, and the other $\phi(v)$ depending on the beam velocity v, it is possible to bring the measured transmissions onto a single curve $P(t) = T/\phi(v)$. This is demonstrated in Fig. 22. The required function $\phi(v)$ is shown in Fig. 23. It has been normalized so as to facilitate comparison with the value $\phi_1(v)$ given by Marion and Young[27] for the probability of Li ions emerging singly charged from a foil.

The fact that the stopping power measured for transmitted $^4HeH^+$ ions (Fig. 19) is almost independent of target thickness is in harmony with the above discussion. It suggests that the internuclear separation does not vary much with dwell time inside the target for those ions that are transmitted and this would account for the ability to separate T into functions of t and v [one would expect $\phi(v)$ to depend rather sensitively upon the internuclear separation].

We have calculated the stopping power for transmitted $^4HeH^+$ using an expression derived by Brandt *et al.*[28]:

$$S_c(t) = (e^2\omega_p^2/v^2)\ln(2mv^2/\hbar\omega_p) \times [Z_1^2 + Z_2^2 + 2Z_1 Z_2 \bar{G}(t)]. \quad (2)$$

Here $\bar{G}(t)$ is a factor describing the average effects over a dwell time t of the interference between the two wakes of the projectiles in a dinuclear cluster. As described above, we believe that the internuclear separation for transmitted ions remains fairly constant inside the target. Also, for these ions, we believe the separation

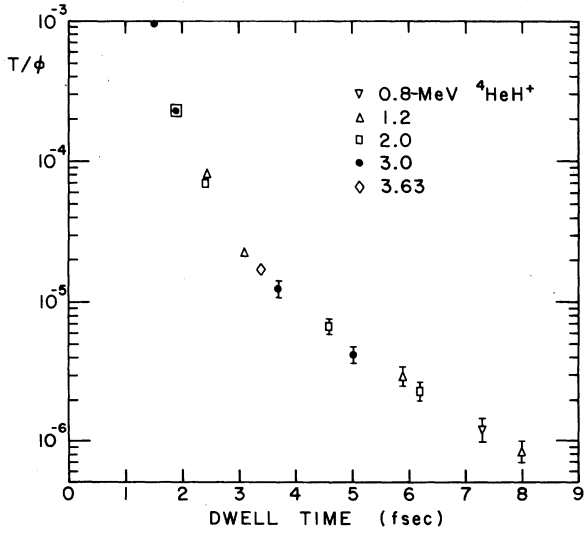

FIG. 22. The transmission yield T (Fig. 17) for $^4HeH^+$ ions divided by $\phi(v)$ is as shown in Fig. 23. The ratio $T/\phi(v)$ is shown plotted as a function of target dwell time.

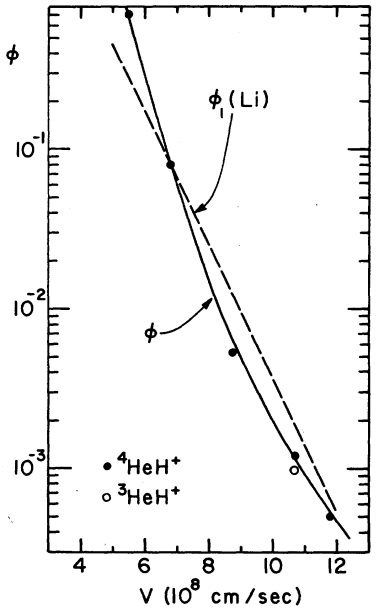

FIG. 23. The function $\phi(v)$ required to bring the transmission yields for HeH^+ onto a single curve (Fig. 22). The value of $\phi(v)$ has been normalized at a $^4HeH^+$ energy of 1.2 MeV to the singly charged fraction $\phi_1(v)$ for lithium ions emerging from a solid (Ref. 27) (dashed line). The solid points are for $^4HeH^+$. The open circle is for 2.4-MeV $^3HeH^+$.

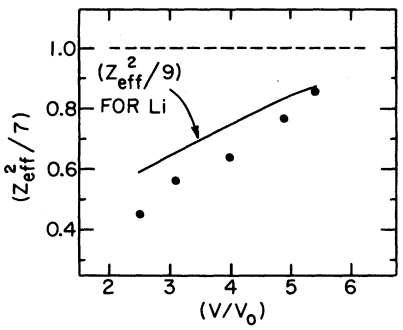

FIG. 24. The normalized effective charge functions for transmitted $^4HeH^+$ ions. The solid line gives the similarly derived result for Li ions. The dashed line represents the limit at high velocities corresponding to fully stripped projectiles.

remains less than the screening distance $a = v/\omega_p$. Under these conditions the predicted value of $\bar{G}$ is about 0.5 and independent of the dwell time. That is, Eq. (2) predicts $S_c = 7\,S_p$, where S_p is the stopping power of a proton having the same velocity as the cluster.

The five data points shown in Fig. 19 for an 8-μg/cm^2 target were fitted with the curve shown, using the expression $S_c = Z^2_{eff} S_p$. The other three curves were obtained by normalization using the ratios of target thicknesses. The ratio $(Z^2_{eff}/7)$ is shown plotted as a function of v in Fig. 24. A similarly derived curve is shown for Li ions, which may be regarded as the united atom ($r = 0$) limit. The fact that the $^4HeH^+$ points lie below the curve for Li presumably reflects a reduced contribution of close collisions to the stopping power at low velocities.

The relation of the widths of the angular distributions for transmitted $^4HeH^+$ ions to the target thickness (Fig. 20) is further evidence suggesting that these ions remain tightly correlated during their passage through the target. (For multiple scattering of monatomic beams, one expects these widths to vary as the square root of the target thickness.)

ACKNOWLEDGMENTS

This research was performed under the auspices of the Division of Basic Energy Sciences of the U. S. Department of Energy. Some of the authors, P. J. Cooney, W. J. Pietsch, and Z. Vager, would like to acknowledge the hospitality at Argonne National Laboratory while this work was in progress.

*Permanent address: Millersville State College, Millersville, Pennsylvania 17551.
†Permanent address: University of Cologne, West Germany.
‡Present address: N. Y. State Dept. of Health, Albany, N. Y. 11201.
§Permanent address: Weizmann Institute of Science, Rehovot, Israel.

[1]D. S. Gemmell, J. Remillieux, J.-C. Poizat, M. J. Gaillard, R. E. Holland, and Z. Vager, Phys. Rev. Lett. 34, 1420 (1975); Nucl. Instrum. Methods 132, 61 (1976).
[2]Z. Vager, D. S. Gemmell, and B. J. Zabransky, Phys. Rev. A 14, 638 (1976).
[3]D. S. Gemmell, Z. Vager, and B. J. Zabransky, Proceedings of 4th Conference on Scientific and Industrial Applications of Small Accelerators, Denton, Texas, October, 1976, IEEE 76CH 1175-9 NPS, p. 329.
[4]E. P. Kanter, P. J. Cooney, D. S. Gemmell, K.-O. Groeneveld, W. J. Pietsch, A. J. Ratkowski, Z. Vager, and B. J. Zabransky, Phys. Rev. A 20, 834 (1979).
[5]D. S. Gemmell, *Radiation Research (Proceedings of the Sixth International Congress of Radiation Research, Tokyo, Japan, May, 1979)*, edited by S. Okada, M. Imamura, T. Terashima, and H. Yamaguchi (University of Tokyo, Tokyo, 1979), pp. 132–144.

[6]D. S. Gemmell, Nucl. Instrum. Methods 170, 41 (1980).
[7]W. J. Pietsch, D. S. Gemmell, P. J. Cooney, E. P. Kanter, D. Kurath, A. J. Ratkowski, Z. Vager, and B. J. Zabransky, Nucl. Instrum. Methods 170, 61 (1980).
[8]P. J. Cooney, D. S. Gemmell, E. P. Kanter, W. J. Pietsch, and B. J. Zabransky, Nucl. Instrum. Methods 170, 73 (1980).
[9]D. S. Gemmell, E. P. Kanter, and W. J. Pietsch, Nucl. Instrum. Methods 170, 79 (1980).
[10]D. S. Gemmell, P. J. Cooney, and E. P. Kanter, Nucl. Instrum. Methods 170, 81 (1980).
[11]E. P. Kanter, P. J. Cooney, D. S. Gemmell, Z. Vager, W. J. Pietsch, and B. J. Zabransky, Nucl. Instrum. Methods 170, 87 (1980).
[12]Z. Vager and D. S. Gemmell, Phys. Rev. Lett. 37, 1352 (1976).
[13]N. Cue, N. V. De Castro Faria, M. J. Gaillard, J.-C. Poizat, and J. Remillieux, Nucl. Instrum. Methods 170, 67 (1980).
[14]W. Kolos and J. M. Peek, Chem. Phys. 12, 381 (1976).
[15]N. Bohr, K. Dan. Vidensk. Selsk. Mat.-Fys. Medd. 18, No. 8, 1 (1948).
[16]J. Neufeld and R. H. Ritchie, Phys. Rev. 98, 1632 (1955); J. Neufeld and R. H. Ritchie, Phys. Rev. 99, 1125 (1955).
[17]M. H. Day, Phys. Rev. B 12, 514 (1975).
[18]M. Kitagawa and Y. H. Ohtsuki, Phys. Rev. B 16, 5321 (1977).
[19]R. Laubert and F. K. Chen, Phys. Rev. Lett. 40, 174 (1978).
[20]R. H. Ritchie, P. M. Echenique, W. Brandt, and B. Basbas, IEEE Trans. Nucl. Sci. NS-26, 1001 (1979).
[21]A. Faibis, R. Kaim, I. Plesser, and Z. Vager, Nucl. Instrum. Methods 170, 99 (1980).
[22]The helium-ion charge-state ratios are taken from the work of J. C. Armstrong, J. V. Mullendore, W. R. Harris, and J. B. Marian, Proc. Phys. Soc. London 86, 1283 (1965).
[23]J.-C. Poizat and J. Remillieux, Phys. Lett. 34A, 53 (1971).
[24]M. J. Gaillard, J.-C. Poizat, A. J. Ratkowski, and J. Remillieux, Nucl. Instrum. Methods 132, 69 (1976).
[25]W. Brandt, R. Laubert, and A. J. Ratkowski, Nucl. Instrum. Methods 132, 57 (1976).
[26]W. Brandt and R. H. Ritchie, Nucl. Instrum. Methods 132, 43 (1976).
[27]*Nuclear Reaction Analysis*, J. B. Marion and F. C. Young (North-Holland, Amsterdam, 1968), p. 38.
[28]W. Brandt, A. Ratkowski, and R. H. Ritchie, Phys. Rev. Lett. 33, 1325 (1974).